~~CONFIDENTIAL~~

Copy

RM A57E21

RESEARCH MEMORANDUM

AERODYNAMIC LOADS ON TAILS AT HIGH ANGLES OF ATTACK AND SIDESLIP

By

J. Richard Spahr

Ames Aeronautical Laboratory
Moffett Field, Calif.

and

Edward C. Polhamus

Langley Aeronautical Laboratory
Langley Field, Virginia

CLASSIFIED DOCUMENT

NATIONAL ADVISORY COMMITTEE
FOR AERONAUTICS

WASHINGTON

July 23, 1957

~~CONFIDENTIAL~~

NACA RM A57E21

NATIONAL ADVISORY COMMITTEE FOR AERONAUTICS

RESEARCH MEMORANDUM

AERODYNAMIC LOADS ON TAILS AT HIGH ANGLES OF ATTACK AND SIDESLIP

By J. Richard Spahr and Edward C. Polhamus

SUMMARY

Results are presented for the loads and moments acting on the individual tail surfaces of a body-tail combination over a wide range of angles of attack and sideslip. The effects of forebody length and panel-panel interference on the characteristics are included. It is shown that large nonlinear variations in these loads and moments, which occur at some combinations of angle of attack and sideslip, cannot be predicted by low-angle theory. A relatively simple, but general, theoretical method for calculating these load and moment characteristics is described, and the results from this method are found to be in good agreement with experiment provided the initial positions of the forebody vortices are known.

It is shown that a simple application of slender-body theory can be used to predict the side loads due to sideslip that are contributed by a vertical tail on a wide variety of wing-body-tail combinations at low angles of attack. For several configurations, changes are indicated which reduced the vertical-tail loads per unit yawing moment of each complete configuration at large angles of attack.

Some results are presented on the effect of high angle of attack on the induced-flow field and tail loads due to a wing at supersonic speed.

INTRODUCTION

Airplanes and missiles are frequently required to operate over a wide range of angles of attack and sideslip. The aerodynamic loading on most aircraft configurations at small angles of attack and sideslip can be adequately predicted by linearized theories. However, at combined angles where either the angle of attack or sideslip is large, serious nonlinearities in the load characteristics occur for which no general theoretical method has heretofore been developed. The results of

reference 1 have shown that, at subsonic Mach numbers, such nonlinearities in the tail loads are caused by the effects of the body and wing vortices and that these effects can be estimated if the strength and positions of the vortices are known.

The purpose of this paper is threefold: (1) to summarize the results at supersonic Mach numbers of recent fundamental and systematic measurements of the loads and moments on the exposed panels of body-panel combinations through a wide range of angles of attack and sideslip; (2) to present a general theoretical method for calculating these load characteristics at any Mach number, which requires only a knowledge of the initial positions of the forebody vortices; and (3) to show the influence of several configuration changes in reducing the vertical-tail loads required for a given yawing moment of the configuration.

SYMBOLS

a maximum body radius

b wing span

c local chord

$\bar{c}$ mean aerodynamic chord

c_n section normal-force coefficient

C_b bending-moment coefficient, $\dfrac{\text{bending moment about root of exposed panel}}{2qSs_v}$

C_h hinge-moment coefficient, $\dfrac{\text{hinge moment about centroid of exposed panel}}{2qS\bar{c}}$

C_n yawing-moment coefficient of configuration

$C_{N,t}$ normal-force coefficient on exposed vertical tail, $\dfrac{\text{normal force}}{qS}$

C_N normal-force coefficient on tail in presence of wing

C_{N_∞} normal-force coefficient on tail alone

C_Y side-force coefficient, $\frac{\text{side force on vertical panel}}{2qS}$.

ΔC_Y change in side-force coefficient of configuration due to wing or vertical tail

Δi_t total differential horizontal-tail incidence

M free-stream Mach number

q free-stream dynamic pressure

s spanwise distance from body center to panel tip

s_v span of one exposed panel

S area of one exposed panel

V free-stream velocity

Z' vertical coordinate with origin at tail-body juncture

α angle of attack, radians unless otherwise specified

β angle of sideslip

ϵ semiapex angle of plan form

ϵ' angle of average downwash acting over span of tail

Subscripts

U upper panel

L lower panel

V due to body vortices

W wing alone

DISCUSSION

Basic Panel-Load Characteristics

The loads and moments acting on the individual lifting surfaces of a cruciform combination are considered first. These surfaces can be considered wing panels of a body-wing-tail combination or the tail surfaces of a wingless configuration. Systematic wind-tunnel tests of the configuration shown in figure 1 have been made at the Ames Aeronautical Laboratory to measure the forces and moments acting on the four individual panels over a wide range of combined angles of attack and sideslip. Representative results of these tests are presented in figure 2 in which the loads and moments acting on the upper and lower vertical panels are given for combined angles of attack and sideslip. The coefficients of side force C_Y on each panel and hinge moment about the panel centroid C_h are shown as functions of sideslip angle β for angles of attack of 0° and 20°. It is seen that the effect of angle of attack on the lower panel is to increase progressively the force while the hinge moment remains unchanged. In contrast, the load and hinge moment on the upper panel are both decreased by angle of attack. The important characteristic to note here is that this decrease is not proportional to angle of sideslip but reaches a maximum at low values of sideslip and results in a large rearward shift in the panel center of pressure and a highly nonlinear variation of the loads and moments on this panel with angle of sideslip. It is this loss in load on the upper vertical panel when serving as a tail fin which is one of the causes of the serious decay in directional stability of most airplanes at large angles of attack. It is apparent that this undesirable characteristic can be alleviated by the use of a lower vertical (ventral) fin, because such a surface does not lose effectiveness with angle of attack but actually gains effectiveness. Results for the panel root bending moment are presented in figure 3. The bending-moment results in conjunction with the side-force results show that the lateral center of pressure of the lower panel remains fixed with changes in angle of attack, whereas that of the upper panel moves outboard with an increase in angle of attack. It is apparent from symmetry that the results of figures 2 and 3 apply directly to horizontal panels if the angles of attack and sideslip are interchanged. The left-hand curves apply to the left horizontal panel and the right-hand curves apply to the right panel.

Consider now the basic cause of these effects of cross coupling between angle of attack and sideslip. The loading due to sideslip on a vertical panel in the presence of a body varies with angle of attack because of two different effects: (1) the change in effective sweepback of the panel and, (2) the change in the influence of the forebody vortices on the panel loading.

Consider, first, the sweepback effect. It can be shown by use of slender-body theory that the lift effectiveness of a wing panel in the

presence of a body decreases with increasing sweepback as in the case of a wing alone. This effect is illustrated in figure 4 which shows the side view of the vertical panels in combination with the body at an arbitrary angle of attack and sideslip. The effect of angle of attack is to increase the leading-edge sweepback of the upper panel and to decrease the sweepback of the lower panel. The resulting changes in the loading due to sideslip over each wing panel is indicated in the right-hand sketch of figure 4. Here, it is shown that the symmetrical spanwise load distribution at zero angle of attack is changed to an asymmetrical distribution at positive angle of attack. The loading on the lower panel is increased and that on the upper panel is decreased.

Consider next the second factor influencing the panel loads at combined angles of attack and sideslip, that is, the influence of the forebody vortices. At moderate and large angles of attack or sideslip, the flow over a body is characterized by a pair of symmetrically disposed vortices on the leeward side caused by crossflow separation. The presence of a vortex in the vicinity of a wing or tail surface changes the loading on the surface by virtue of the induced flow field created by the vortex. Two critical conditions are indicated in figure 5 for which a vortex passes close to one panel and thus has the greatest effect on the loading: first, the combination of high angle of attack and low sideslip in which the upper panel is primarily affected by the vortex and, second, high sideslip and low angle of attack in which the left panel is most affected. It will be recalled from figure 2 that these were the two conditions for which the largest nonlinear changes in panel loading occurred. The effect of a vortex on the panel loads is illustrated by the sketches in figure 5 which show the changes in the spanwise load distribution, from strip theory, due to a vortex passing near the tip of each panel. It is observed that, above the vortex on the upper panel, a loading to the left occurs and below the vortex a loading to the right occurs. This loading corresponds to the distribution of sidewash induced by the vortex along the span of the panels. The magnitude of the loading increases with the strength of the vortex and decreases with the distance of the vortex from the panel. With the vortex located near the tip of the panel, the net force due to the vortex is to the right and reduces the load and bending moment existing on the panel without the vortex present. If the vortex is moved toward the body, its effect on the net panel load would diminish, because the two regions of opposite loading would become more nearly compensating.

Expressions based on simple theoretical concepts have been derived for the prediction of the forces and moments acting on a panel at arbitrary angles of attack and sideslip in which the effects of both sweepback and body vortices have been taken into account. These expressions are illustrated in figure 6 which gives the equations for the side force acting on the two vertical panels at a given sideslip angle. The first term in each of these expressions represents the side force at zero angle of attack; the second term represents the effect of sweepback due to angle of attack; and the last term represents the contribution of the

forebody separation vortices. The factor C_{Y_W} is the side force of the panel alone at zero angle of attack and is evaluated from experiment, where available, or from a suitable wing theory. The factors K_W and K_ϕ are both computed by slender-body theory and, for a circular body, depend only on the ratio of the body radius a to the panel semispan s as shown by the curves in figure 6. It is observed that K_W increases from 1 to 2 as the configuration changes from an all-wing configuration to a body with no wings. The factor K_ϕ, on the other hand, increases to a maximum for combinations with relatively small bodies and then decreases to zero as the wings vanish. It is also noted that, because of panel-panel interference, K_ϕ is larger for the planar configuration than for the cruciform arrangement, but that this effect becomes smaller as a/s increases. Although the factors K_W and K_ϕ have been computed from slender-body theory, these equations are not necessarily restricted to combinations having slender panels because K_W and K_ϕ are simply load ratios which modify the load on a vertical-tail panel alone to take into account the presence of the body and of the angle of attack. The theoretical and experimental comparisons of Nielsen and Kaattari (ref. 2) have established the validity of the factor K_W for essentially any plan form or aspect ratio.

The importance of the panel leading-edge sweepback on the side force is seen from the equations in figure 6 where $\tan \epsilon$, which is proportional to the aspect ratio for a triangular plan form, appears in the denominator. Thus, the lower the aspect ratio the larger the effect of angle of attack on the vertical panel loads due to sideslip.

The evaluation of the last terms in these equations requires the computation of the effect of each of the forebody vortices and their images on the wing-panel loading. The strength and paths of these vortices have been calculated by means of a stepwise procedure based on incompressible vortex theory. Such calculations, however, require a knowledge of the normal-force distribution along the forebody and the initial vortex position. The work of Jorgensen and Perkins (ref. 3) has demonstrated the validity of this method for bodies of circular cross section, and subsequent work has indicated its applicability to bodies of arbitrary cross section. The calculation of the effect of a vortex of known strength and position on the loading of a wing panel in the presence of a body is made most simply by means of strip theory. In the application of the strip theory, it is assumed that the strength and path of each vortex remain unchanged by the addition of the wing panel to the body. The downwash for an ideal vortex is then calculated, and the additional spanwise load distribution due to the vortex flow field is computed. The lifting effectiveness of each longitudinal strip is taken as the two-dimensional value for a wing having the same leading-edge sweepback. An alternate method, based on slender-body theory, is currently being investigated at the Ames Aeronautical Laboratory for the calculation of the

effects of a vortex on a wing panel in the presence of a body. In this method the influence of the wing-panel flow field on the vortex paths is taken into account and, thus, one of the assumptions of the strip-theory method is avoided. Preliminary results of this study indicate that the effects of such changes in the vortex path on the wing load may be important for plan forms of low aspect ratio.

Calculations have been made by means of these theoretical methods to predict the experimental panel-load characteristics discussed earlier. Figure 7 shows a comparison between experiment and theory at an angle of attack of 20° for the variation of side force and hinge moment with sideslip angle for the two vertical panels.

In addition to the experimental values shown by the symbols, three theoretical curves are shown in each case to illustrate the importance of the two aerodynamic effects just discussed: first, a low-angle theory, given by the first term in the equations of figure 6; second, the theory including the sweepback effect, given by the first two terms; and, third, the theory including both the sweepback and vortex effects (based on the experimental initial vortex positions), as given by the complete equations. It is seen from these comparisons that the load characteristics of either panel can be predicted adequately by the complete theory. It is noted that for the lower panel the vortex effect is negligible because the body vortices are a relatively large distance from this panel. (See fig. 5.)

The effects of forebody length on the vertical-panel loads are indicated in figure 8. In this figure is presented a comparison of the load characteristics of the original combination with a combination having one-half the original forebody length. The importance of forebody length is evident from this comparison which shows that this change in the forebody virtually eliminates the nonlinearities due to the body vortices. This result is caused by the reduction in the vortex strength and by the inboard movement of the vortices, both of which tend to reduce the effect of the vortices as pointed out earlier. These experimental results are in good agreement with those predicted by the theoretical method.

The effects of the presence of adjacent surfaces on the loads acting on a wing or tail surface are illustrated in figure 9. In this figure is shown the variation of the side force of each vertical panel with angle of sideslip at a high angle of attack in the presence of each of the other panels of a cruciform arrangement. These curves show that the addition of the opposite vertical or the left horizontal panel has no effect on the loads of either vertical panel, but the addition of the right horizontal panel increases the load on the lower panel and decreases the load on the upper panel. These panel-panel interference effects are associated partly with the cross coupling of the sidewash velocities in potential flow and partly with interference effects of the forebody vortex flow.

The loads on the tail surfaces of complete configurations at zero or small angles of attack are considered next. Under these conditions, the side load contributed by a wing or tail surface to an arbitrary configuration at any sideslip angle or Mach number can be computed by means of a simple theoretical method. In this method the side-force contribution of a vertical-tail surface is given by the product of the side force acting on the surface alone and an interference factor which is a function only of the cross-sectional shape of the combination at the tail location. Slender-body theory in conjunction with apparent-mass relationships are used to evaluate this interference factor for a given configuration. This theoretical method has been used to predict the side-force characteristics of a number of current aircraft configurations shown in figure 10, for which such experimental information was available. Most of these configurations represent recent fighter airplanes and include a wide variety of wing-body-tail arrangements. In addition, a research model from the National Advisory Committee for Aeronautics is included. The cross-sectional arrangements used in the theoretical calculations to approximate the actual configurations are shown in figure 11. The correlation between experiment and theory is given in terms of the change in side force due to the addition of the surface designated by the solid line in each of the sketches. The results for subsonic speeds are indicated by the flagged symbols and those for supersonic speeds by the plain symbols. Although the change in side force ΔC_Y shown in this figure includes the load induced on the body by the surface, the load on the surface itself can also be calculated by the theoretical method. The good agreement shown here between experiment and theory for such a wide variety of configurations at both subsonic and supersonic speeds shows the general usefulness of the theoretical method in the prediction of side loads and vertical-tail loads due to sideslip at small angles of attack where in some cases these loads are maximum.

The effects of angle of attack on the tail loads of wing-body-tail combinations are now considered. Figure 12 presents some results obtained at the Langley Aeronautical Laboratory which show the effect of angle of attack on the spanwise load distribution due to sideslip on the vertical tail of an airplane configuration having a low, midposition, or high wing at a Mach number of 0.8. It is observed that in all cases an increase in angle of attack causes an increase in the loading along the outer portion of the span and a decrease near the root. From the previous discussions it can be recognized that this effect is associated with the forebody crossflow separation vortices. It can also be noted by comparing the low- and high-wing results that the effect of wing height is considerably greater at an angle of attack of 15° than at an angle of attack of 0°; thus, an effect of wing position on the forebody vortices is indicated. Figure 13 shows similar results for a Mach number of 1.4 but, in this case, the effects of angle of attack and wing height are somewhat less.

Effect of Directional Stability

This paper so far has dealt with methods of estimating wing or tail loads and comparisons of the vertical-tail loads encountered by various configurations for a given sideslip angle where it has been shown that for conventional configurations the vertical-tail load generally decreases with angle of attack. This reduction in tail load is, however, usually accompanied by a loss in directional stability which results in larger sideslip angles being encountered before the restoring moment necessary to counteract a given disturbance is developed. If, as in the usual case, the wing-fuselage combination is directionally unstable, then the increased sideslip angle would require more tail load to counteract the instability of the wing-fuselage combination and the total tail load would increase with angle of attack despite the fact that the tail load per unit sideslip decreased with angle of attack. However, if the wing-fuselage combination has neutral directional stability throughout the angle-of-attack range, the vertical-tail load would (if any variation of carryover to the body with angle of attack is neglected) be independent of the over-all directional stability. Unfortunately, the instability of the wing-fuselage combination often increases with angle of attack (see ref. 4) and results in an increase in the vertical-tail loads encountered.

In view of the importance of the wing-fuselage directional stability characteristics, it is the purpose of this portion of the paper to illustrate the effect, on the vertical-tail load per unit restoring moment, of several wing-fuselage-configuration changes which appear attractive from stability considerations. Figures 14 to 16 illustrate the effect of stability by presenting, as a function of angle of attack, the vertical-tail-load coefficient for a unit yawing-moment coefficient of the complete configuration. Inasmuch as the only purpose of these figures is to indicate the effect of angle of attack and compare changes to a given configuration, and since the wing areas and spans and moment reference points are involved when making comparison between different configurations, the scales have been omitted. One such change is the use of narrow horizontal strips, or strakes, on the fuselage forebody to alleviate the loss in directional stability with angle of attack. (See ref. 5.) The effect that these strakes have on the measured load of the exposed vertical tail per unit yawing moment of the complete configuration are shown in figure 14 for a Mach number of 0.6. The strakes had spans equal to 10 percent of the maximum fuselage diameter and extended over the front 27 percent of the fuselage. The wing, which had an aspect-ratio-4 delta plan form clipped to an aspect ratio of 3, differed from that in reference 5 and was selected because, for this wing, the strakes also provide a beneficial effect on the longitudinal stability characteristics. The strake-off condition is represented by the circular symbols and it can be observed that the tail load per unit yawing moment increases rapidly. With the strakes on (denoted by square symbols), however, the vertical-tail load decreases with angle of attack

and is considerably less than that for the basic configuration. This rather large improvement is associated with a reduction in the wing-fuselage instability at the higher angles of attack.

The effect of a change in fuselage-afterbody shape on the vertical-tail loads, as indicated by the tail contribution to side force, is presented in figure 15 for a Mach number of 2.0. Two configurations were investigated, one having a circular afterbody and the other having an elliptical afterbody. Both fuselages had the same volume and the same longitudinal distribution of cross-sectional area. The elliptical afterbody is used as an attempt to reduce the fuselage instability over the entire angle-of-attack range while maintaining the necessary fuselage volume. The desired stability results were obtained and were accompanied by large reductions in the vertical-tail load for a given yawing moment. This is illustrated by the two variations with angle of attack. The solid curve represents the tail load for the configuration with the circular afterbody, and the dashed curve represents the tail load for the elliptical-afterbody configuration. The results indicate a large reduction in the tail load over the entire angle-of-attack range. This reduction in vertical-tail load results from the decrease in fuselage instability and a transfer of load from the tail to the fuselage afterbody which may, in many cases, be a desirable trade.

The effect of wing height on the vertical-tail loads at a Mach number of 2.9 is shown in figure 16. In this figure are shown the tail-load results (as indicated by the tail contribution to side force) for a configuration having a triangular wing of aspect ratio 4 in a low and high position as indicated in the upper left-hand sketch. From a comparison of these curves, it is observed that raising the wing from the low to high position effects a significant reduction in the tail loads, especially at large angles of attack. This reduction is caused by the influence of the wing pressure field acting on the body as indicated in the sketches on the right. As pointed out earlier, the normal force on the right panel is greater than that on the left panel, and thus a lateral pressure difference across the body is created by the wing. It is apparent that the difference in the positive pressures from the high wing causes an increase in the body side force and, hence, a stabilizing moment, but that the low wing produces a decrease in side force. The yawing moment induced by the low wing is small because of the short moment arm. Thus, the favorable effect of a high wing on the tail loads is the result of the improvement in the tail-off directional stability. In the estimation of tail bending moments, however, the adverse effect of a high wing on the span loading, as previously pointed out, must be considered.

Effect of Lateral Control

One lateral-control device which has been found to induce rather large loads on the vertical tail is the differentially deflected horizontal tail. This device is illustrated in figure 17 where the measured normal force induced on the exposed portion of the vertical tail by a differentially deflected horizontal tail is presented (denoted by the square symbols) as a function of Mach number. The vertical-tail loads presented for the differentially deflected horizontal tail were obtained at zero sideslip with a total differential deflection of 30° (right down 15°, left up 15°). These deflections produce a positive roll and a wing-tip helix of approximately 0.07 throughout the Mach number range investigated. The vertical-tail load, which, of course, occurs only instantaneously as the roll control is applied, increases rather rapidly with Mach number and approximately doubles between a Mach number of 0.6 and 0.9. Although experimental results are not available for supersonic speeds, theoretical considerations of the effect of Mach number on the effectiveness of the horizontal and vertical tails and the amount of vertical-tail area within the Mach cone from the horizontal tail indicate that a rather rapid reduction in the vertical-tail load might be expected at supersonic speeds. It would appear, therefore, that the maximum loads induced on the vertical tail probably occur at high subsonic speeds. In order to give a better indication of the magnitude of the normal force induced on the vertical tail, the normal force encountered at an angle of sideslip of 6° with no differential deflection of the horizontal tail is presented by the circular symbols as a function of Mach number for comparison. This comparison indicates that at high subsonic speeds vertical-tail normal forces corresponding to an angle of sideslip of approximately 7° are induced by a total differential deflection of 30° of the horizontal tail.

Effects of Wing on Horizontal-Tail Loads

The influence of a wing on the horizontal-tail-load characteristics at two angles of attack is indicated in figures 18 and 19. In these figures are shown some recent wind-tunnel results for the induced flow field behind a rectangular wing at zero sideslip and the influence of this flow field on the load acting on a rectangular horizontal-tail surface. The local downwash and sidewash angles, dynamic pressure, and Mach number were surveyed in a vertical plane at the tail location. In these figures the variations in downwash and in the tail load are shown as functions of the tail height in wing chords. The tail normal force C_N is computed from the average downwash, dynamic pressure, and Mach number existing at the tail plane. The results for an angle of attack of 6° (fig. 18) show that, when the tail is located between the two trailing-edge waves, the average downwash is small, that is, $1 - \frac{\epsilon'}{\alpha}$ is nearly 1, and the loss in tail load is small, that is, the lift ratio is close to 1. The effect of the viscous

wake from the blunt trailing edge of the wing is evidenced by the variations in this region directly behind the trailing edge. If the tail surface passes through either of the trailing-edge waves, a sudden downwash occurs which actually reverses the load on the tail, a situation obviously to be avoided. As the tail is raised farther above the wing plane, the downwash diminishes to zero and the tail load returns to its free-stream value at the point for which the tail is located at the shock wave from the wing leading edge. Similarly, the curves for negative values of tail height would be expected to return to free-stream conditions when the tail passes below the lower shock wave from the wing leading edge. The close agreement of the downwash and tail-load curves is an indication of the small deviations in the average dynamic pressure and Mach number in the wake from their free-stream values at this angle of attack. The results for an angle of attack of 20° (fig. 19) also show a sudden downwash and loss in tail load as the tail moves through the upper wave from the wing trailing edge. However, it is noted that, in contrast to the results for an angle of attack of 6°, the tail-load curves do not follow the downwash curves in the rest of the wake, and despite the increase in downwash below the wing, the tail load is preserved. This effect results from changes in dynamic pressure and Mach number in the wing wake at this angle of attack and demonstrates the necessity of taking into account these changes in the prediction of loads on both horizontal- and vertical-tail surfaces behind a wing at large angles of attack.

CONCLUDING REMARKS

The results of wind-tunnel tests have shown that variations in the loads and moments on a lifting surface in the presence of a body can exhibit large nonlinearities at combined angles of attack and sideslip which cannot be predicted by low-angle theory. A relatively simple, but general, theoretical method for calculating these loads under such conditions has been described in which both the effects of leading-edge sweepback and of the forebody vortex flow are taken into account. This calculative method, however, requires a knowledge of the initial positions of the forebody vortices. It was found that the results of this theoretical method were in good agreement with experiment. Results have been presented which show the effects of forebody length and panel-panel interference on the load characteristics. It was demonstrated that a simple application of slender-body theory could be used successfully to predict the side loads contributed by a vertical tail on a wide variety of wing-body-tail combinations at small angles of attack and at both subsonic and supersonic Mach numbers.

For three configurations, changes were described which reduced the vertical-tail loads required for a given yawing moment of each complete configuration at large angles of attack. These were (1) addition of

horizontal strakes along the forebody, (2) change in the afterbody cross-sectional shape from circular to elliptical in which the major axis is vertical, and (3) movement of the wing from a low to a high position.

Ames Aeronautical Laboratory
National Advisory Committee for Aeronautics
Moffett Field, Calif., Mar. 4, 1957

REFERENCES

1. Kuhn, Richard E., Hallissy, Joseph M., Jr., and Stone, Ralph W., Jr.: A Discussion of Recent Wind-Tunnel Studies Related to the Problem of Estimating Vertical- and Horizontal-Tail Loads. NACA RM L55E16a, 1955.

2. Nielsen, Jack N., and Kaattari, George E.: Method for Estimating Lift Interference of Wing-Body Combination at Supersonic Speeds. NACA RM A51J04, 1951.

3. Jorgensen, Leland H., and Perkins, Edward W.: Investigation of Some Wake Vortex Characteristics of an Inclined Ogive-Cylinder Body at Mach Number 1.98. NACA RM A55E31, 1955.

4. Polhamus, Edward C., and Hallissy, Joseph M., Jr.: Effect of Airplane Configuration on Static Stability at Subsonic and Transonic Speeds. NACA RM L56A09a, 1956.

5. Sleeman, William C., Jr.: Investigation at High Subsonic Speeds of the Effects of Various Horizontal Fuselage Forebody Fins on the Directional and Longitudinal Stability of a Complete Model Having a 45° Sweptback Wing. NACA RM L56J25, 1957.

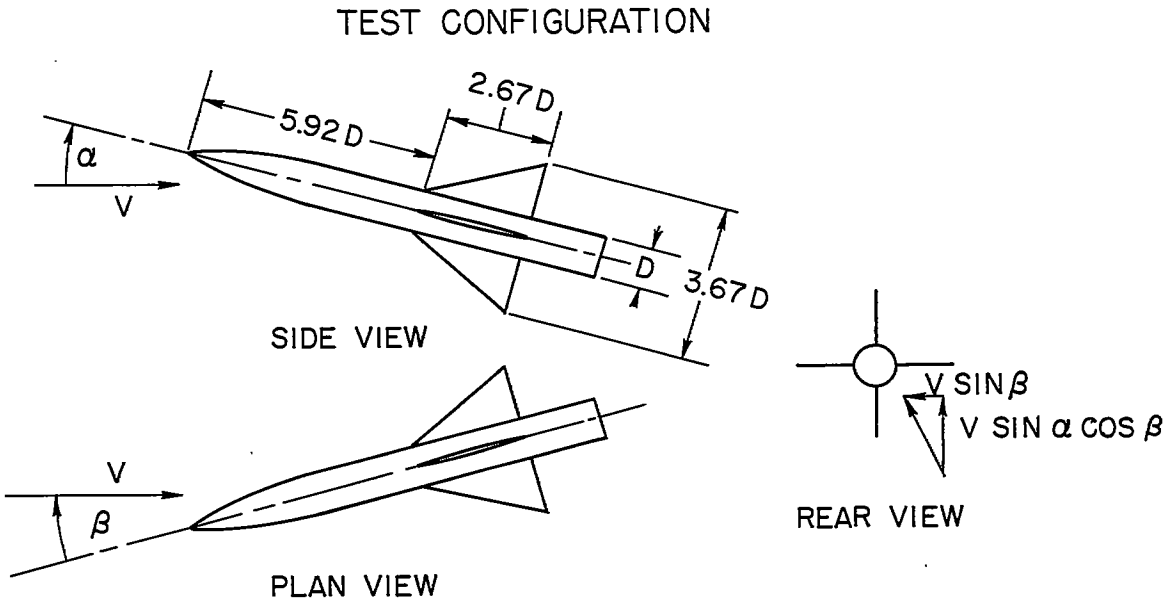

Figure 1

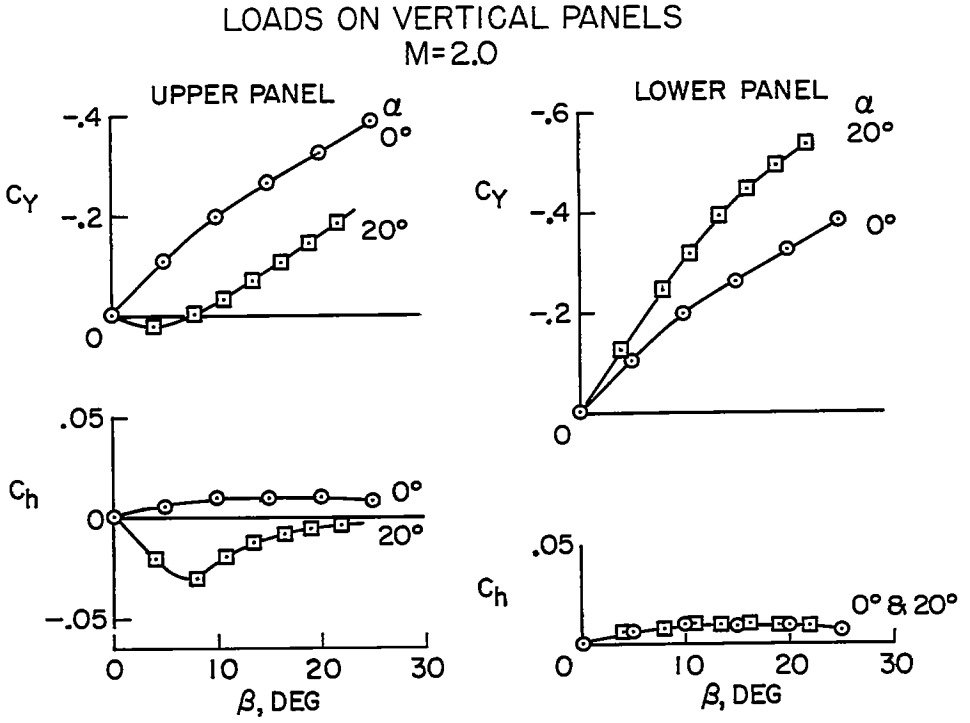

Figure 2

BENDING MOMENTS ON VERTICAL-TAIL PANELS
M = 2.0

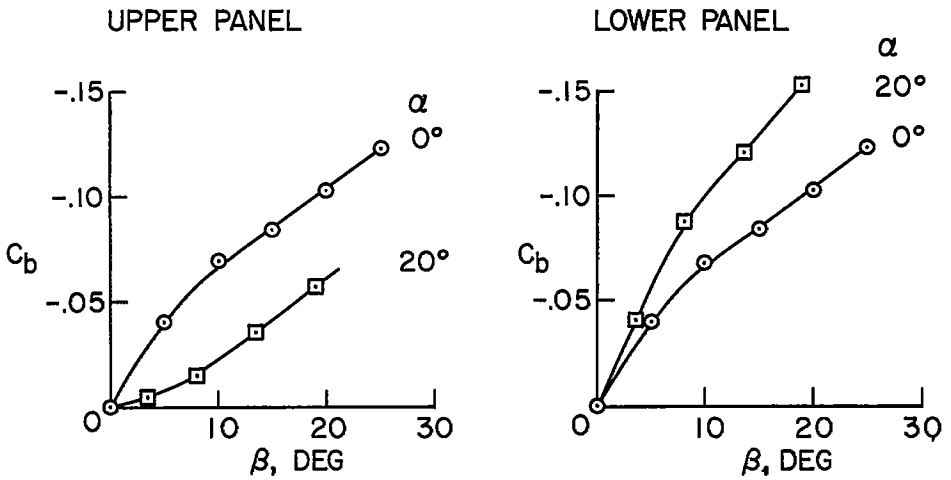

Figure 3

EFFECT OF ANGLE OF ATTACK ON LOADING
DUE TO SIDESLIP

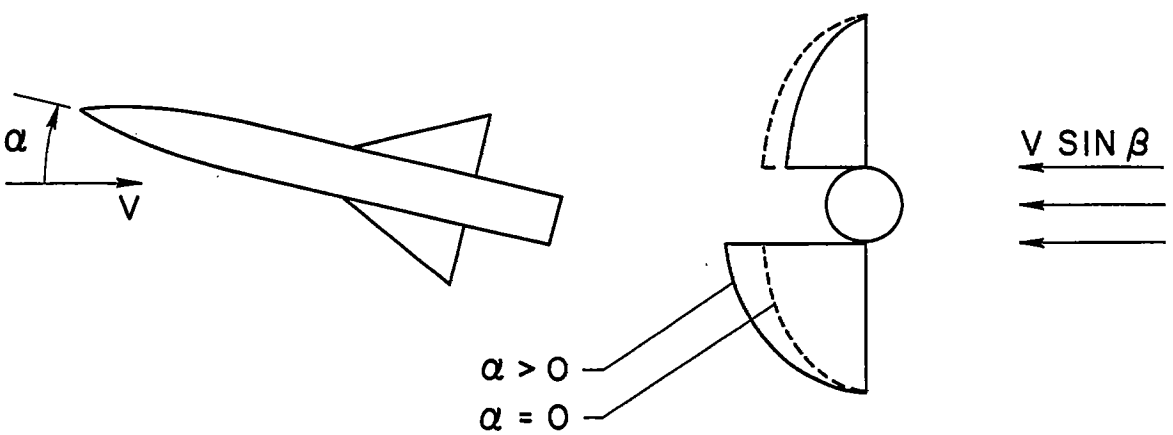

Figure 4

EFFECT OF FOREBODY VORTICES

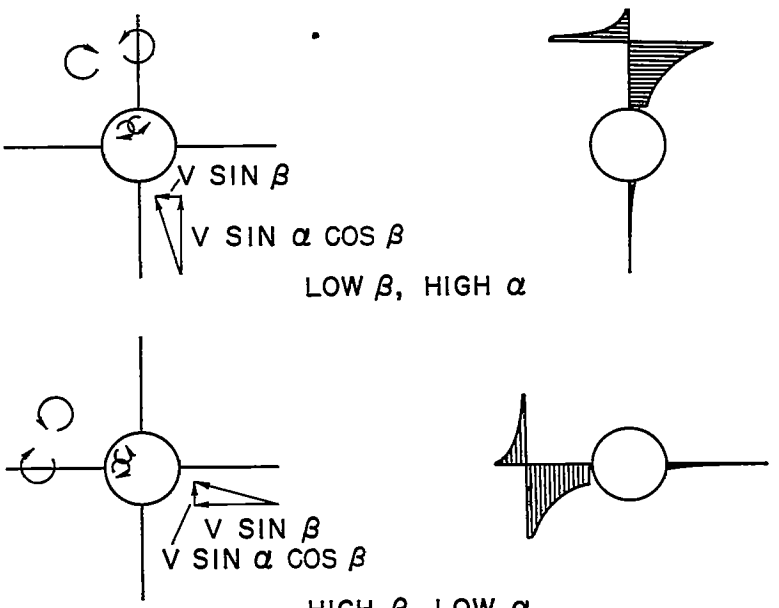

Figure 5

PANEL FORCES FOR COMBINED α AND β

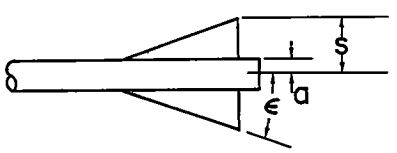

$$C_{Y_U} = C_{Y_W}\left(K_W - \frac{K_\phi}{\tan \epsilon}\alpha\right) + C_{Y_{V_U}}$$

$$C_{Y_L} = C_{Y_W}\left(K_W + \frac{K_\phi}{\tan \epsilon}\alpha\right) + C_{Y_{V_L}}$$

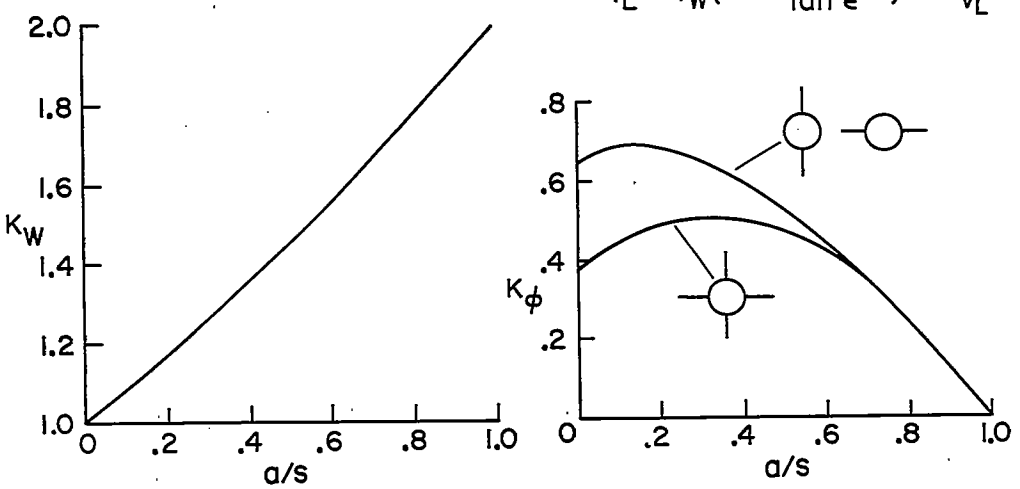

Figure 6

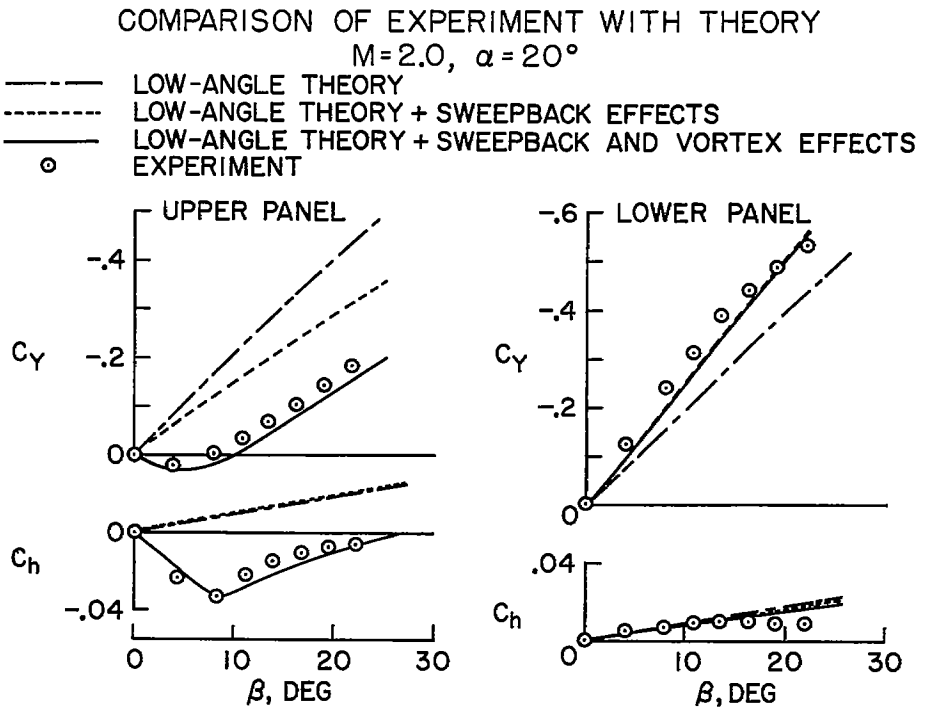

Figure 7

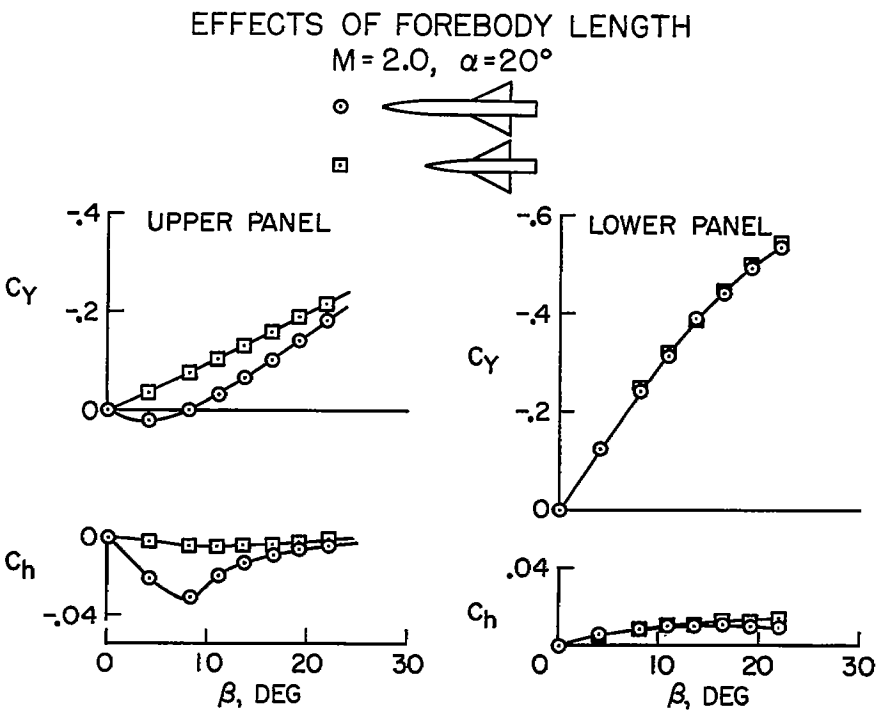

Figure 8

EFFECTS OF PANEL-PANEL INTERFERENCE
M=2.0; α=20°

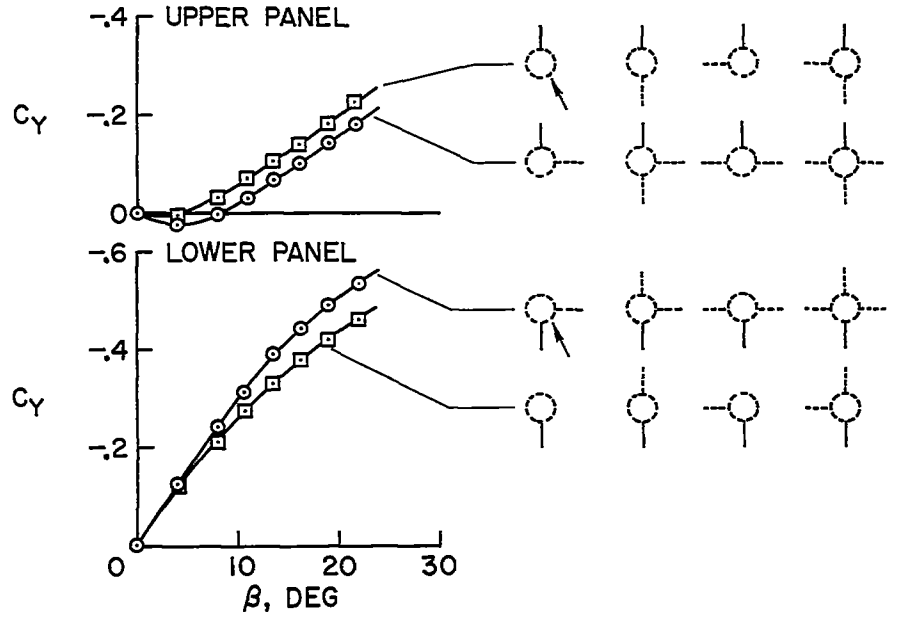

Figure 9

CONFIGURATIONS STUDIED

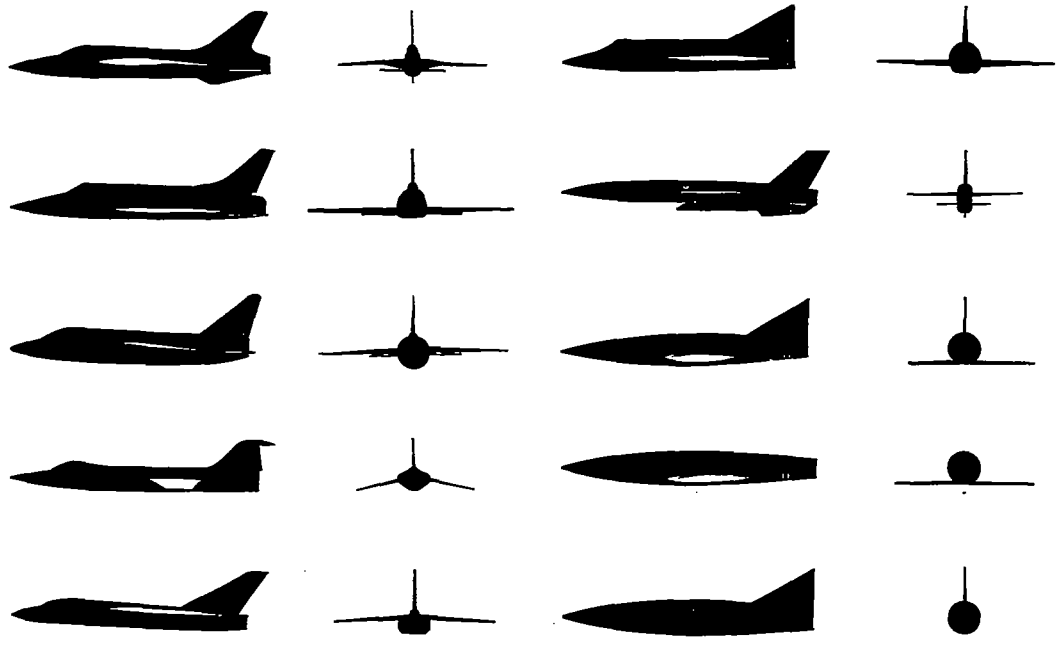

Figure 10

SIDE-LOAD CORRELATION FOR SMALL ANGLE OF ATTACK

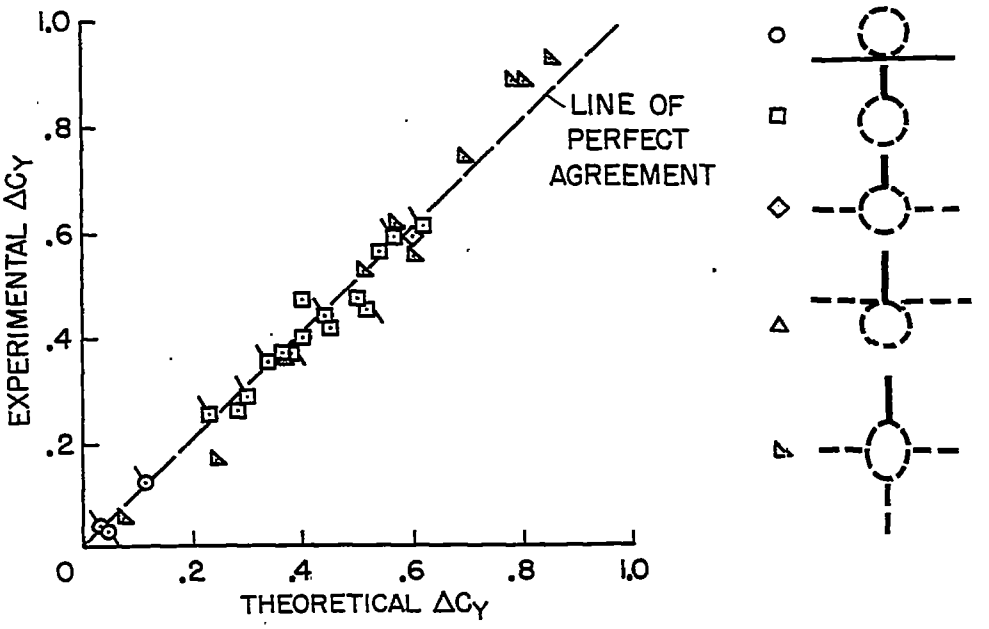

Figure 11

EFFECT OF WING HEIGHT ON VERTICAL-TAIL LOADING

$M = 0.8$; $\beta = 5°$

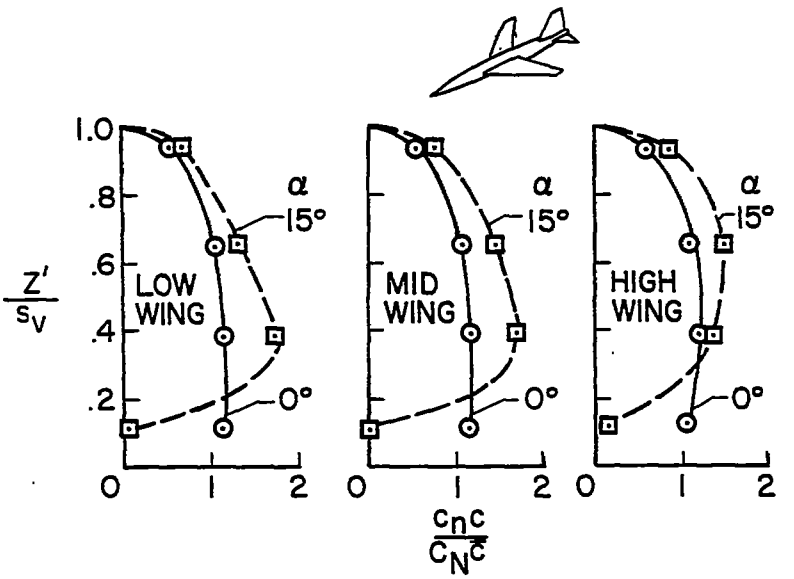

Figure 12

EFFECT OF WING HEIGHT ON VERTICAL-TAIL LOADING

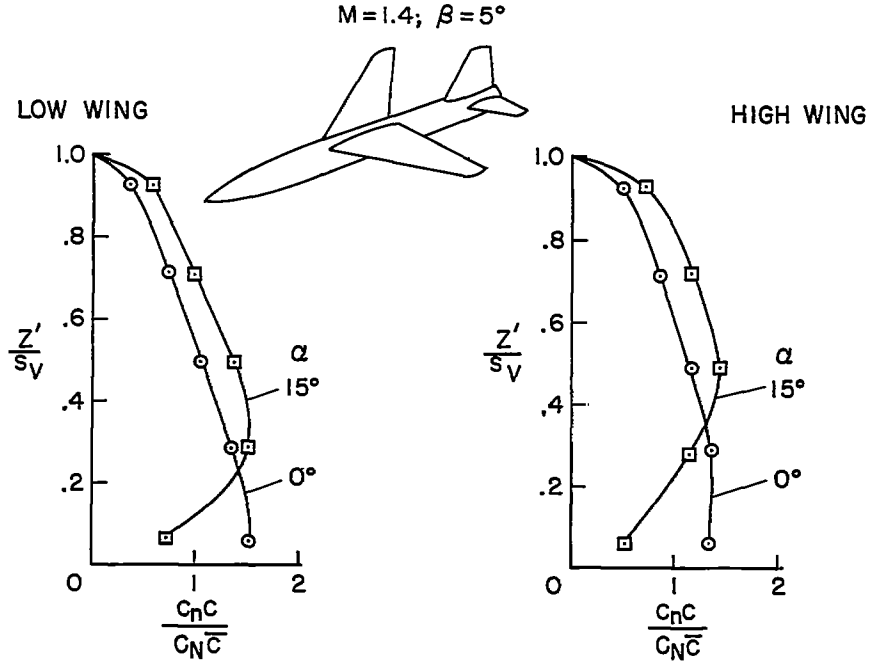

Figure 13

EFFECT OF FUSELAGE STRAKES ON VERTICAL-TAIL LOAD

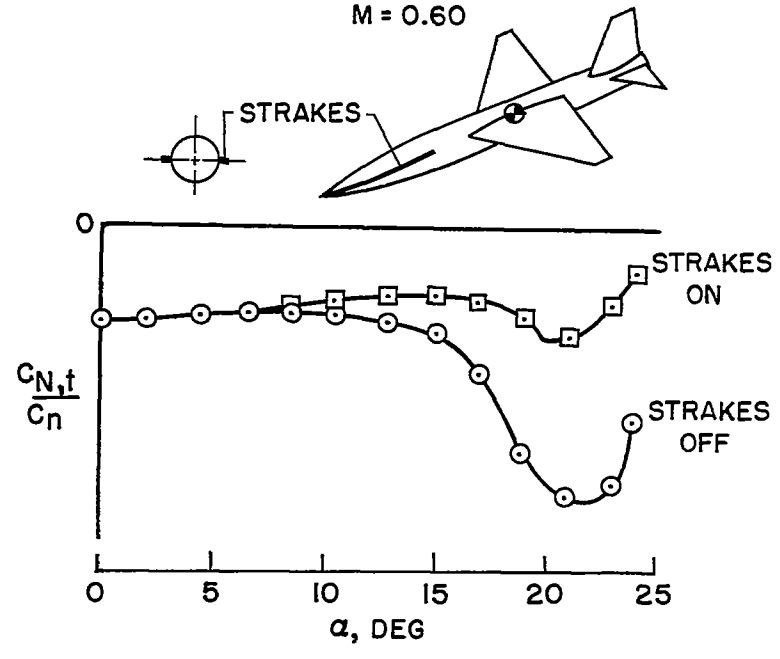

Figure 14

EFFECT OF AFTERBODY SHAPE ON VERTICAL-TAIL LOAD
M=2.0

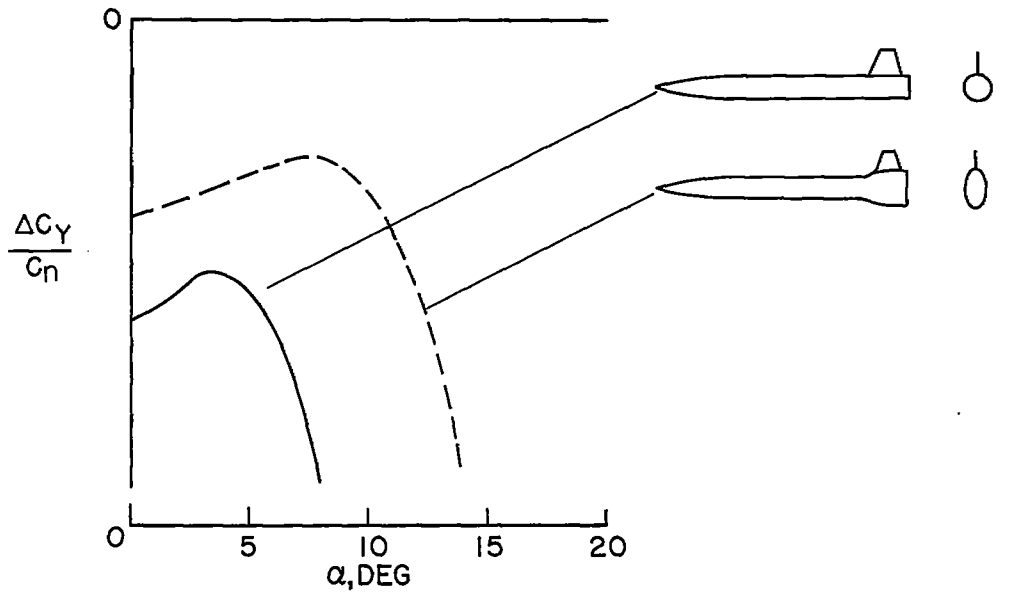

Figure 15

EFFECT OF WING HEIGHT ON SIDE-FORCE DUE TO VERTICAL TAIL M=2.9

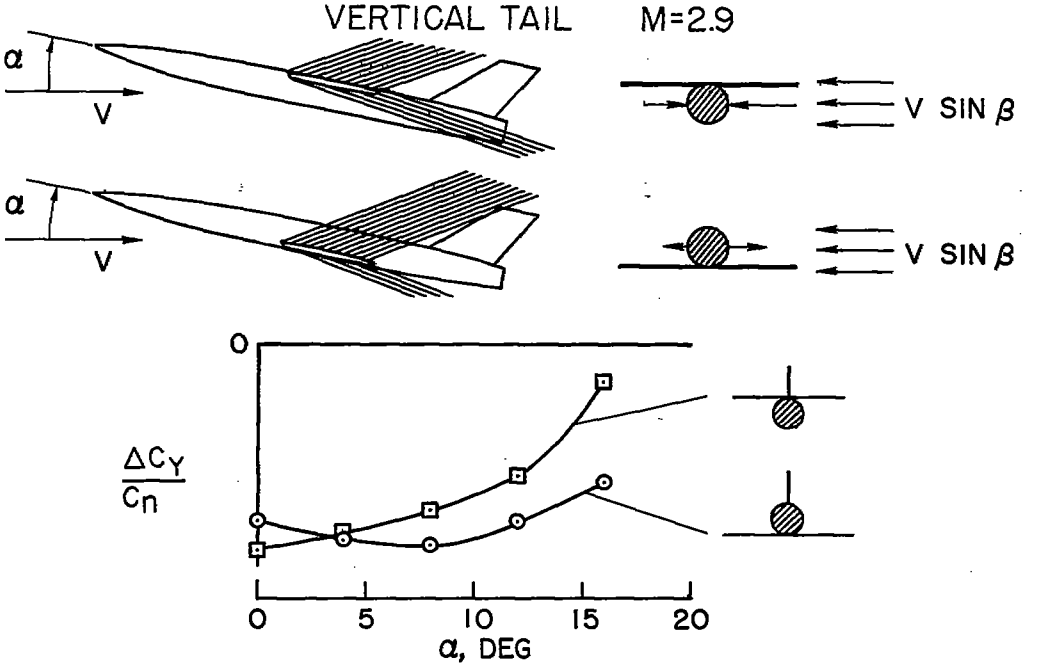

Figure 16

EFFECT OF TAIL ROLL CONTROL ON VERTICAL-TAIL LOAD

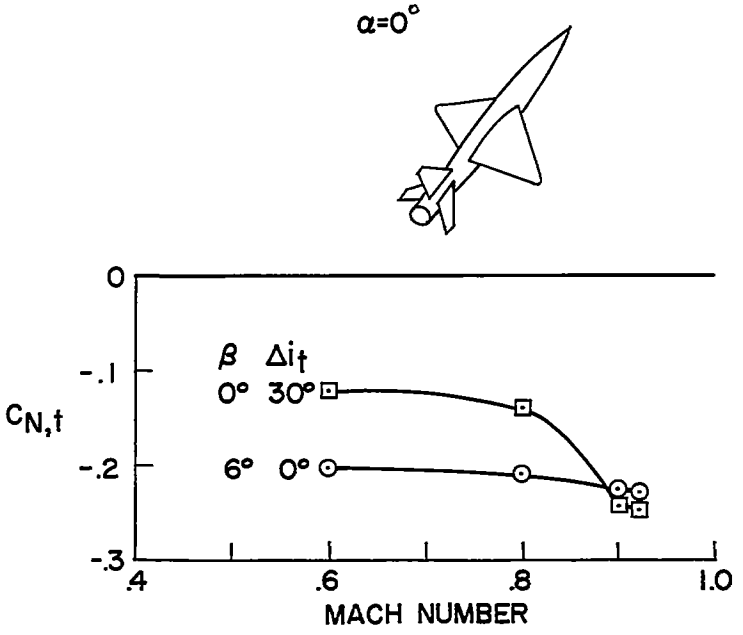

Figure 17

EFFECT OF WING ON TAIL LOADS
M=2.46; β=0°; α=6°

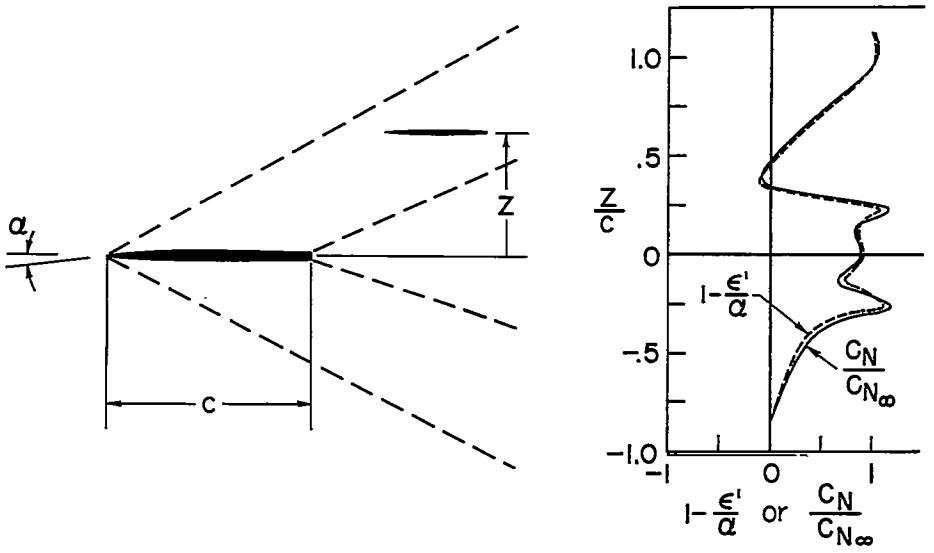

Figure 18

EFFECT OF WING ON TAIL LOADS
M=2.46; β=0°; α=20°

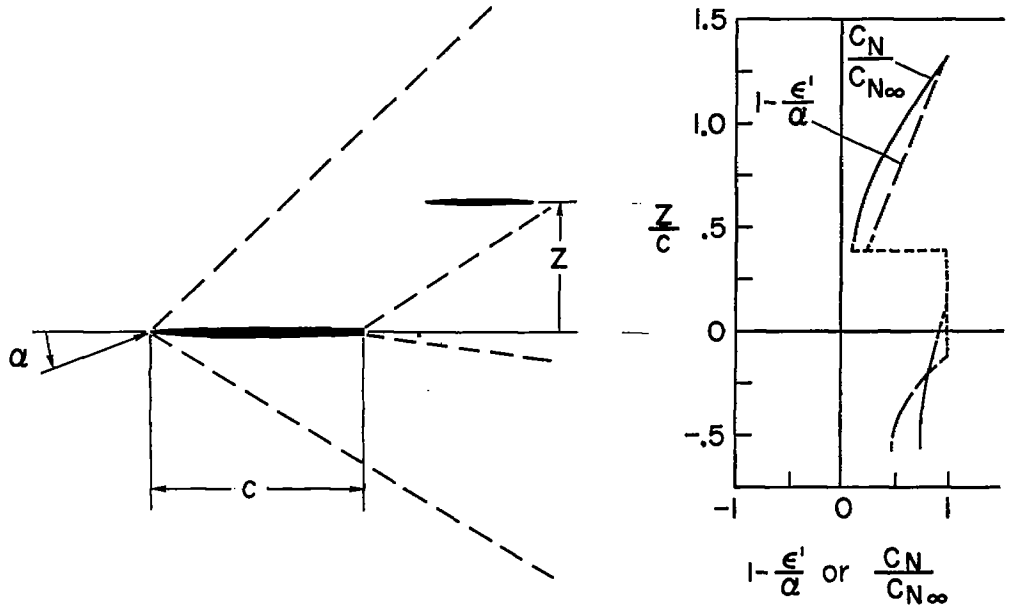

Figure 19

NACA - Langley Field, Va.